

RECEIVED: May 19, 2025

ACCEPTED: August 8, 2025

PUBLISHED: November 13, 2025

Measurement of the phase between strong and electromagnetic amplitudes in the decay $J/\psi \rightarrow \phi\eta$



The BESIII collaboration

E-mail: besiii-publications@ihep.ac.cn

ABSTRACT: The first direct measurement of the relative phase between the strong and electromagnetic amplitudes for a J/ψ decaying into a vector-pseudoscalar final state is performed using 26 energy points of e^+e^- annihilation data between 3.00 GeV and 3.12 GeV. The data sets were collected by the BESIII detector with a total integrated luminosity of 452 pb^{-1} . By investigating the interference pattern in the cross section lineshape of $e^+e^- \rightarrow \phi\eta$, the relative phase between the strong and electromagnetic amplitudes of J/ψ decay is determined to be within $[133^\circ, 228^\circ]$ at 68% confidence level.

KEYWORDS: e^+e^- Experiments, Particle and Resonance Production, QCD

ARXIV EPRINT: [2505.05888](https://arxiv.org/abs/2505.05888)

JHEP11(2025)077

Contents

1	Introduction	1
2	BESIII experiment and data sets	2
3	Event selection and background analysis	3
4	Observed cross section of $e^+e^- \rightarrow \phi\eta$	4
4.1	Signal yield	4
4.2	Efficiency determination	6
4.3	Systematic uncertainty	6
5	Cross section lineshape of $e^+e^- \rightarrow \phi\eta$	8
6	Summary	11
The BESIII collaboration		15

1 Introduction

At center-of-mass (CM) energies in the vicinity of the J/ψ resonance, the annihilation of e^+e^- into hadronic final states can be described in terms of three amplitudes [1]: J/ψ production followed by the purely strong decay of the J/ψ meson (mediated by 3 gluons), denoted as \mathcal{A}_{3g} , the purely electromagnetic (EM) decay of the J/ψ meson (mediated by a virtual photon), denoted as \mathcal{A}_γ , and the continuum Quantum Electrodynamic (QED) process, denoted as $\mathcal{A}_{\text{cont}}$, as shown in figure 1. \mathcal{A}_{3g} and \mathcal{A}_γ proceed via $e^+e^- \rightarrow$ virtual photon $\rightarrow J/\psi \rightarrow f$, while the continuum QED process is direct $e^+e^- \rightarrow$ virtual photon $\rightarrow f$. The relative phase $\phi_{\gamma,3g}$ between the strong and EM amplitudes for the hadronic decays of the J/ψ can be directly determined by analyzing the interference pattern in the cross section lineshape of the produced particles as a function of the CM energy, \sqrt{s} . The total Born cross section for the $e^+e^- \rightarrow f$ process can be expressed as:

$$\sigma_f(s) \propto |\mathcal{A}_{\text{cont}}(s) + [\mathcal{A}_\gamma(s) + \mathcal{A}_{3g}(s) \cdot e^{i\phi_{\gamma,3g}}] \cdot e^{i\phi_{\text{cont},\gamma}}|^2, \quad (1.1)$$

where $\phi_{\text{cont},\gamma}$ is the relative phase between EM and continuum processes, and it is determined to be 0° by analyzing the interference patterns in the cross section lineshapes of $J/\psi \rightarrow e^+e^-$, $J/\psi \rightarrow \mu^+\mu^-$, and $J/\psi \rightarrow \eta\pi^+\pi^-$ processes [1–4]. The process of $J/\psi \rightarrow \eta\pi^+\pi^-$ violates G-parity conservation and proceeds purely through electromagnetic decay. Assuming $\phi_{\text{cont},\gamma} = 0^\circ$, the total cross section of $e^+e^- \rightarrow f$ in the vicinity of the J/ψ resonance can be recast as:

$$\sigma_f(s) \propto |\mathcal{A}_{\text{cont}}(s) + \mathcal{A}_\gamma(s) + \mathcal{A}_{3g}(s) \cdot e^{i\phi_{\gamma,3g}}|^2. \quad (1.2)$$

Thus far, no existing theory has provided a satisfactory explanation for the origin or implications of $\phi_{\gamma,3g}$. Experimentally, model-dependent analyses, which rely on SU(3) flavor

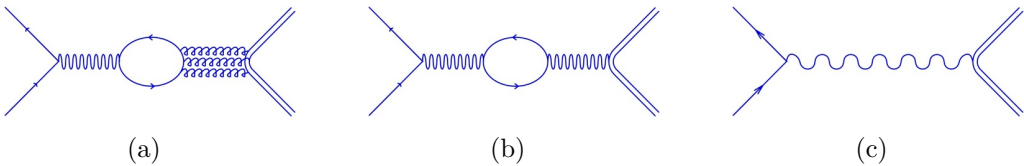


Figure 1. The three classes of diagrams for $e^+e^- \rightarrow \phi\eta$ in the vicinity of a charmonium resonance [1]. The charmonium state is represented by a charm quark loop. (a) Charmonium strong decay via 3 gluons. (b) Charmonium EM decay via a virtual photon. (c) The continuum process via a virtual photon.

symmetry and symmetry breaking of light quarks, observe $\phi_{\gamma,3g}$ to be around 90° using J/ψ two-body decays into meson pairs with quantum numbers (J^P) of 1^-0^- [5, 6], 0^-0^- [7, 8], 1^-1^- [8], and 1^+0^- [9], and for J/ψ decays into $N\bar{N}$ baryon pairs [10, 11]. Similar model-dependent analyses suggest $\psi(2S)$ decays to pairs of mesons with 0^-0^- also have $\phi_{\gamma,3g}$ around 90° [12], but $\psi(2S)$ decays to pairs of mesons with 1^-0^- and 1^+0^- are found to have a value of $\phi_{\gamma,3g}$ around 0° [9]. BESIII recently determined $\phi_{\gamma,3g}$ for the J/ψ in the $e^+e^- \rightarrow 5\pi$ multi-hadron process to be $(84.9 \pm 3.6)^\circ$ or $(-84.7 \pm 3.1)^\circ$, which is model independent [1]. More research is needed to understand the difference between J/ψ and $\psi(2S)$ decays. In addition, experimental results can be used to provide more constraints on QCD calculations.

Until now, there has been no model-independent measurement of $\phi_{\gamma,3g}$ in the decay of the J/ψ into vector-pseudoscalar (VP) mesons. The scan data collected around the J/ψ resonance by the BESIII detector provides a unique opportunity for the direct phase measurement of J/ψ decays. In this analysis, we measure $\phi_{\gamma,3g}$ in the process $J/\psi \rightarrow \phi\eta$ by analyzing the interference pattern in the cross section lineshape of $e^+e^- \rightarrow \phi\eta$ directly for the first time.

2 BESIII experiment and data sets

The BESIII detector [13] records symmetric e^+e^- collisions provided by the BEPCII storage ring [14], which operates with the CM energy range from $\sqrt{s} = 1.85$ GeV to 4.95 GeV, with a peak luminosity of $1.1 \times 10^{33} \text{ cm}^{-2} \text{ s}^{-1}$ achieved at $\sqrt{s} = 3.773$ GeV. BESIII has collected large data samples in this energy region [15–17]. The cylindrical core of the BESIII detector covers 93% of the full solid angle and consists of a helium-based multilayer drift chamber (MDC), a plastic scintillator time-of-flight system (TOF), and a CsI(Tl) electromagnetic calorimeter (EMC), which are all enclosed in a superconducting solenoidal magnet providing a 1.0 T magnetic field. The solenoid is supported by an octagonal flux return yoke with resistive plate counter muon-identification modules interleaved with steel. The charged-particle momentum resolution at $1 \text{ GeV}/c$ is 0.5%, and the resolution of the rate of energy loss, dE/dx , is 6% for electrons from Bhabha scattering. The EMC measures photon energies with a resolution of 2.5% (5.0%) at 1 GeV in the barrel (end-cap) region. The time resolution in the TOF barrel region is 68 ps, while that in the end-cap region is 110 ps. The end-cap TOF system was upgraded in 2015 using multigap resistive plate chamber technology, providing a time resolution of 60 ps [18–20].

In this analysis, the data samples collected in 2012, 2015, 2018, and 2019 at 26 different CM energies with a total integrated luminosity of about 452 pb^{-1} are used. The CM energies and the integrated luminosities of each data sample are summarized in table 1. The CM

energies are measured by the Beam Energy Measurement System (BEMS), in which photons from a CO₂ laser are Compton back scattered off the electron beam and detected by a high-purity Germanium detector [21]. The integrated luminosities are determined using $e^+e^- \rightarrow \gamma\gamma$ events [22].

Monte Carlo (MC) simulated data samples produced with a GEANT4-based software package [23], which includes the geometric description of the BESIII detector and the detector response, are used to determine reconstruction efficiencies and to estimate backgrounds. The simulation models the beam energy spread and initial state radiation (ISR) in the e^+e^- annihilation with the generator KKMC [24, 25]. An MC sample of J/ψ inclusive decays is used to explore possible hadronic backgrounds. In this sample, the production of the J/ψ resonance is simulated by the generator KKMC [24, 25]. The known decay modes of the J/ψ are generated with EVTGEN [26, 27] incorporating branching fractions from the Particle Data Group (PDG) [28] and the remaining unknown decays are generated according to the LUNDCHARM [29] model. Radiation from charged final state particles is incorporated using the PHOTOS program [30]. The signal MC samples for the $e^+e^- \rightarrow \phi\eta$ process at each energy point, generated using P-waves in the production process with the CONEXC generator [31], which accounts for the vacuum polarization and radiative effects up to next-to-leading order, are used to estimate the reconstruction efficiency. The beam energy spread is incorporated in all MC samples. We correct the helix parameters of charged kaons to reduce the difference between simulated and data samples [32]. The ϕ mesons are generated with invariant masses up to 1.08 GeV/ c^2 . This range of $0.98 < M_\phi < 1.08$ GeV/ c^2 is used as a definition of the ϕ signal reported in this paper [33].

3 Event selection and background analysis

To select $e^+e^- \rightarrow \phi\eta$ events, ϕ and η candidates are reconstructed through their K^+K^- and $\gamma\gamma$ decay modes, respectively. Candidate events are required to have at least two candidate charged kaons with opposite charge and at least two candidate photons.

Charged kaons detected by the MDC are required to be within the MDC acceptance of $|\cos\theta| < 0.93$, where θ is the polar angle with respect to the symmetry axis of the MDC, and their distance of closest approach to the interaction point is required to be within 10 cm along the beam direction and 1 cm in the transverse plane. For each charged track, particle identification (PID) is implemented with the specific ionization energy loss (dE/dx) measured by the MDC and the time of flight recorded by the TOF. The combined confidence levels for kaon and pion hypotheses (CL_π and CL_K) are calculated. A kaon is identified by requiring $CL_K > 0.001$ and $CL_K > CL_\pi$.

Photon candidates are reconstructed by showers in the EMC. The photon candidates are required to be in the barrel region ($|\cos\theta| < 0.80$) of the EMC with at least 25 MeV of energy deposition, and in the endcap region ($0.86 < |\cos\theta| < 0.92$) with at least 50 MeV of energy deposition. To exclude showers induced by the charged tracks, the opening angle between a candidate shower and the closest charged track must be greater than 10°. To suppress electronic noise and showers unrelated to the candidate event, the difference between the EMC time and the event start time is required to be within [0, 700] ns.

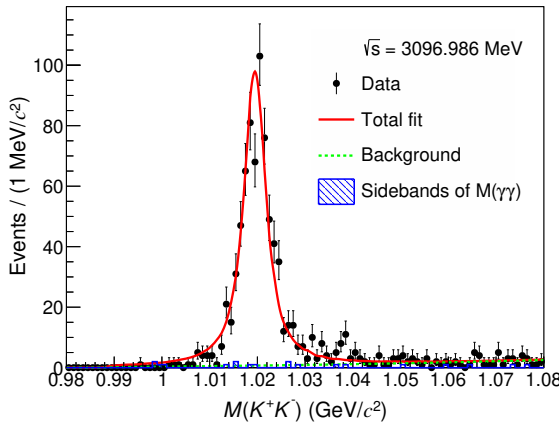


Figure 2. Fit to the $M(K^+K^-)$ distribution at $\sqrt{s} = 3096.986$ MeV. The black dots with error bars are candidate events in the η mass window of $M(\gamma\gamma)$. The red solid curve is the fit result. The green dotted line is the fitted background shape. The blue histogram is the $M(K^+K^-)$ spectrum for candidate events in the $s\eta$ sidebands of $M(\gamma\gamma)$.

A four-constraint (4C) kinematic fit is applied under the hypothesis $e^+e^- \rightarrow K^+K^-\gamma\gamma$, constraining the measured four-momenta of all particles to the four-momentum of the e^+e^- system. For each event, the $K^+K^-\gamma\gamma$ combination with the least χ^2_{4C} is retained for further study. Events with $\chi^2_{4C} > 85$ are rejected.

To further suppress background, a requirement on the invariant mass of the $\gamma\gamma$ system, $M(\gamma\gamma)$, is applied, $|M(\gamma\gamma) - M_\eta| < 30$ MeV/ c^2 , where M_η is the nominal η mass [28] and 30 MeV/ c^2 corresponds to 3 times the detector resolution in the measurement of $M(\gamma\gamma)$. After applying the above selection criteria, the yield of $e^+e^- \rightarrow \phi\eta$ candidates is determined by fitting the invariant mass spectrum of the K^+K^- system, $M(K^+K^-)$, in the range $0.98 < M(K^+K^-) < 1.08$ GeV/ c^2 . Potential peaking backgrounds from non- η ϕ processes in the $M(K^+K^-)$ spectrum are analyzed using candidate events in the sidebands of $M(\gamma\gamma)$, $60 < |M(\gamma\gamma) - M_\eta| < 90$ MeV/ c^2 . An example of this background in the data sample at $\sqrt{s} = 3096.986$ MeV is illustrated by the blue histogram in figure 2. It is negligible for each energy point.

4 Observed cross section of $e^+e^- \rightarrow \phi\eta$

The observed cross section is calculated with

$$\sigma_{\phi\eta}^{\text{obs}} = \frac{N_{\text{sig}}}{\mathcal{L} \cdot \varepsilon \cdot \mathcal{B}}, \quad (4.1)$$

where N_{sig} is the yield of observed signal events, \mathcal{L} is the integrated luminosity, ε is the detection efficiency, and $\mathcal{B} = \mathcal{B}(\phi \rightarrow K^+K^-) \cdot \mathcal{B}(\eta \rightarrow \gamma\gamma) = (19.3 \pm 0.2)\%$ is the product of branching fractions for the $\phi \rightarrow K^+K^-$ and $\eta \rightarrow \gamma\gamma$ decays quoted from the PDG [28].

4.1 Signal yield

The number of signal $e^+e^- \rightarrow \phi\eta$ events is determined by an unbinned maximum-likelihood fit to the $M(K^+K^-)$ spectrum. The signal is modeled by an MC-simulated shape. The background is described with an ARGUS function [34], with the endpoint set to the kinematic

\sqrt{s} (MeV)	\mathcal{L} (pb $^{-1}$)	N_{sig}	ε (%)	$\sigma_{\phi\eta}^{\text{obs}}$ (pb)
3000.00 \pm 0.20	15.85 \pm 0.11	25.7 $^{+5.6}_{-4.9}$	36.3 \pm 0.2	23.1 $^{+5.0}_{-4.4}$
3020.00 \pm 0.20	17.32 \pm 0.12	22.0 $^{+5.1}_{-4.3}$	36.9 \pm 0.2	17.7 $^{+4.1}_{-3.5}$
3049.66 \pm 0.03	14.92 \pm 0.16	20.0 $^{+4.8}_{-4.2}$	37.3 \pm 0.2	18.5 $^{+4.5}_{-3.9}$
3058.71 \pm 0.03	15.06 \pm 0.16	28.0 $^{+5.6}_{-5.0}$	37.5 \pm 0.2	25.6 $^{+5.2}_{-4.6}$
3080.00 \pm 0.20	293.42 \pm 0.95	497.3 $^{+24.1}_{-23.4}$	37.5 \pm 0.2	23.3 $^{+1.2}_{-1.1}$
3082.51 \pm 0.04	4.77 \pm 0.06	7.1 $^{+3.1}_{-2.4}$	37.9 \pm 0.2	20.4 $^{+8.9}_{-7.0}$
3087.59 \pm 0.13	2.47 \pm 0.02	8.0 $^{+3.2}_{-2.5}$	38.1 \pm 0.2	44.1 $^{+17.5}_{-13.8}$
3088.87 \pm 0.02	15.56 \pm 0.17	28.3 $^{+6.4}_{-5.7}$	38.0 \pm 0.2	24.8 $^{+5.6}_{-5.0}$
3091.78 \pm 0.03	14.91 \pm 0.16	35.0 $^{+6.3}_{-5.6}$	38.2 \pm 0.2	31.9 $^{+5.8}_{-5.1}$
3094.71 \pm 0.08	2.14 \pm 0.03	34.5 $^{+6.4}_{-5.6}$	39.9 \pm 0.2	209.8 $^{+38.8}_{-34.1}$
3095.45 \pm 0.08	1.82 \pm 0.02	90.9 $^{+10.2}_{-9.8}$	40.1 \pm 0.2	645.7 $^{+72.9}_{-70.6}$
3095.73 \pm 0.08	2.92 \pm 0.02	291.3 $^{+18.4}_{-17.7}$	40.4 \pm 0.2	1277.9 $^{+82.5}_{-79.2}$
3095.84 \pm 0.08	2.14 \pm 0.03	328.4 $^{+19.1}_{-18.5}$	40.2 \pm 0.2	1979.8 $^{+119.8}_{-116.0}$
3096.20 \pm 0.07	4.98 \pm 0.03	827.9 $^{+32.0}_{-31.4}$	41.0 \pm 0.2	2098.2 $^{+85.4}_{-83.9}$
3096.99 \pm 0.08	3.10 \pm 0.02	755.7 $^{+29.9}_{-29.2}$	41.3 \pm 0.2	3054.4 $^{+127.1}_{-124.5}$
3097.23 \pm 0.10	1.68 \pm 0.01	418.1 $^{+22.2}_{-21.6}$	41.9 \pm 0.2	3073.3 $^{+168.0}_{-163.5}$
3097.23 \pm 0.08	2.07 \pm 0.03	473.2 $^{+24.0}_{-23.3}$	41.1 \pm 0.2	2879.4 $^{+154.0}_{-149.9}$
3097.65 \pm 0.08	4.66 \pm 0.03	860.5 $^{+32.2}_{-31.6}$	41.8 \pm 0.2	2286.0 $^{+90.5}_{-88.9}$
3098.36 \pm 0.08	2.20 \pm 0.03	229.8 $^{+17.1}_{-16.2}$	41.1 \pm 0.2	1316.5 $^{+100.4}_{-95.1}$
3098.73 \pm 0.08	5.64 \pm 0.03	335.1 $^{+20.1}_{-19.2}$	41.6 \pm 0.2	737.2 $^{+45.1}_{-43.1}$
3099.06 \pm 0.09	0.76 \pm 0.01	23.0 $^{+5.6}_{-4.9}$	41.0 \pm 0.2	382.4 $^{+93.2}_{-81.7}$
3101.38 \pm 0.11	1.61 \pm 0.02	13.0 $^{+4.0}_{-3.3}$	41.3 \pm 0.2	101.0 $^{+30.8}_{-25.5}$
3104.00 \pm 0.08	5.72 \pm 0.03	53.5 $^{+8.7}_{-8.1}$	41.2 \pm 0.2	117.6 $^{+19.2}_{-17.9}$
3105.60 \pm 0.09	2.11 \pm 0.03	7.8 $^{+3.3}_{-2.6}$	40.4 \pm 0.2	47.4 $^{+19.7}_{-15.9}$
3112.07 \pm 0.09	1.72 \pm 0.02	10.4 $^{+3.9}_{-3.2}$	39.9 \pm 0.2	78.3 $^{+29.3}_{-24.1}$
3119.89 \pm 0.12	1.26 \pm 0.02	3.0 $^{+2.1}_{-1.7}$	38.1 \pm 0.2	32.2 $^{+22.3}_{-15.2}$

Table 1. Summary of the CM energy, luminosity, signal yield, efficiency, and the observed cross section of $e^+e^- \rightarrow \phi\eta$ at each energy point. Statistical uncertainties are quoted for the signal yields, efficiencies, and the observed cross sections, while both statistical and systematic uncertainties are combined in quadrature for the CM energies [1] and luminosity [1, 22].

threshold of twice the K^\pm mass. Due to the low statistics of the data samples, the yield follows a Poisson distribution [35] and cannot be approximated as a Gaussian distribution. Therefore, an asymmetric uncertainty is estimated. An example of the fit result for data at $\sqrt{s} = 3096.986$ MeV is illustrated in figure 2, and the corresponding signal yield for each energy point is presented in table 1.

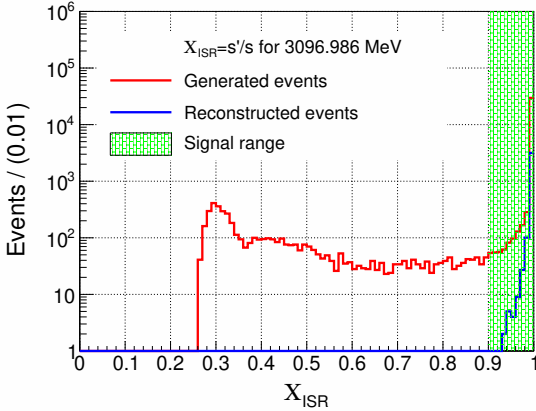


Figure 3. Distribution of $X_{\text{ISR}} = s'/s$ in the signal MC sample at $\sqrt{s} = 3096.986$ MeV. The red (blue) line shows the generated (reconstructed) events. The events in the green shaded region are used to obtain the efficiency.

4.2 Efficiency determination

The reconstruction efficiency at each energy point is obtained based on the signal MC samples simulated with the CONEXC generator [31] and corrected by iteration.

In the CONEXC generator, the precision of simulated events with $X_{\text{ISR}} = s'/s$ depends on the precision of the cross section lineshape of $e^+e^- \rightarrow \phi\eta$ used as input to the generator in the energy range below \sqrt{s} . Here, s represents the squared energy in the CM frame of the e^+e^- system before the emission of ISR photons, and s' represents the squared energy after the emission. In this analysis, the cross section lineshape of $e^+e^- \rightarrow \phi\eta$ obtained by combining the measurements from BaBar [36], BESIII [37], and Belle [38] in the range between the $\phi\eta$ mass threshold and 3.12 GeV is taken as input to the generator. Due to the deviations of the cross section lineshape among different measurements and the complexities arising from the $\phi(1680)$ and $\phi(2170)$ resonances, there is a large uncertainty on the cross section lineshape in the range between the $\phi\eta$ mass threshold and 2.9 GeV. Figure 3 shows the X_{ISR} distribution in the MC sample simulated at $\sqrt{s} = 3096.986$ MeV. Only events with $X_{\text{ISR}} > 0.9$ remain after the 4C kinematic fit. To reduce the uncertainty on the reconstruction efficiency caused by the lineshape, only the simulated events with $X_{\text{ISR}} > 0.9$ are used to estimate the reconstruction efficiency.

Additionally, the cross section lineshape in the range between 3.00 GeV and 3.12 GeV is not precise enough. To reasonably simulate the ISR effect, an iterative MC-generating method as described in refs. [31, 37, 39, 40] is applied. The iteration procedure is repeated until the change in the cross section calculated by eq. (4.1) is less than 0.5%, which is the calculation uncertainty of the CONEXC generator. Finally, the reconstruction efficiency and the $\sigma_{\phi\eta}^{\text{obs}}$ for each energy point are summarized in table 1.

4.3 Systematic uncertainty

Several sources of systematic uncertainties are considered on the observed cross section measurement. These include differences between data and MC simulation for the tracking efficiencies, PID efficiencies, photon reconstruction efficiencies, kinematic fit, mass window

selection of $M(\gamma\gamma)$, iteration procedure, input lineshape, and integrated luminosity measurement. The uncertainties from the fit procedure, and the branching fractions of the intermediate state decays are also considered.

- *Luminosity.* The integrated luminosity is determined using $e^+e^- \rightarrow \gamma\gamma$ events with an uncertainty of 1.0% [22].
- *Branching fractions.* The branching fractions are quoted from the PDG [28]: $\mathcal{B}(\phi \rightarrow K^+K^-)$ is $(49.1 \pm 0.5)\%$, with an uncertainty of 1.0%; and $\mathcal{B}(\eta \rightarrow \gamma\gamma)$ is $(39.36 \pm 0.18)\%$, with an uncertainty of 0.5%.
- *Tracking and PID efficiencies.* The systematic uncertainties of the tracking and PID efficiencies are both assigned as 1.0% per track, determined using a control sample of $e^+e^- \rightarrow K^+K^-\pi^+\pi^-$ events [37].
- *Photon reconstruction.* The systematic uncertainty due to the photon reconstruction is assigned to be 1.0% per photon using a control sample of $J/\psi \rightarrow \pi^+\pi^-\pi^0$ events [37].
- *Kinematic fit.* A helix correction is performed on the kaon tracks [32, 37] to reduce the difference between data and MC samples caused by the kinematic fit for each energy point. The difference between the reconstruction efficiency obtained from the signal MC samples with and without the helix correction is studied for each energy point. The largest deviation, 0.3%, is taken as the systematic uncertainty for all energy points.
- *Iteration procedure.* The systematic uncertainty associated with the iterative procedure is estimated by comparing the difference in the reconstruction efficiency between the last two iterations for each energy point. The largest, 0.2%, is taken as the systematic uncertainty for all energy points.
- *Input lineshape.* During the iteration mentioned in section 4.2, the cross section lineshape of $e^+e^- \rightarrow \phi\eta$ input to the CONEXC generator is obtained by fitting the measured cross sections. The fit parameters, along with their uncertainties, obtained from the last fit iteration are listed in table 3. The uncertainties on these parameters lead to an uncertainty of the efficiency obtained with the lineshape as input in the simulation of the signal MC samples. We sample 100 sets of lineshape parameters $(\phi_{\gamma,3g}, \mathcal{F}, C)$ using the Gaussian Copula method [41] by considering their correlations. With these 100 lineshapes as inputs, 100 sets of the signal MC samples at each energy point are generated. The relative change of efficiency, $\frac{\varepsilon_i - \varepsilon}{\varepsilon}$, is calculated at each energy point, where ε is the nominal efficiency and ε_i is the efficiency obtained from the i^{th} ($i = 1, 2, \dots, 100$) signal MC sample. The $\frac{\varepsilon_i - \varepsilon}{\varepsilon}$ distribution is fitted using a Gaussian function for each energy point. Conservatively, the maximum standard deviation of the Gaussian functions, 1.8%, is taken as the systematic uncertainty on the reconstruction efficiency caused by the input lineshape for all energy points.
- *Mass window of $M(\gamma\gamma)$.* The resolution of the mass of the η peak is determined by fitting the $M(\gamma\gamma)$ spectrum. It is found to be $10 \text{ MeV}/c^2$ and is consistent between data and signal MC samples at each energy point. Therefore, the systematic uncertainty caused by the η mass window in $M(\gamma\gamma)$ is ignored.

- *Fit procedure.* The following three aspects are considered when evaluating the systematic uncertainty associated with the fit procedure. (1) *ϕ fit range.* To study the uncertainty caused by the ϕ fit range, an alternative fit is performed for each energy point by changing the ϕ fit range from $(0.98, 1.08) \text{ GeV}/c^2$ to $(0.98, 1.07) \text{ GeV}/c^2$. (2) *Signal shape.* To study the uncertainty caused by the signal shape, an alternative fit using the MC-simulated shape convolved with a Gaussian function with free parameters is performed for each energy point. (3) *Background shape.* To study the uncertainty caused by the background shape, an alternative fit using an ARGUS function with a floating endpoint is performed for each energy point. For each aspect, the largest change of the signal yield among all energy points is taken as the systematic uncertainty for all energy points.

A summary of all systematic uncertainties is presented in table 2. The sources marked with stars are common and correlated systematic uncertainties for different energy points and are from the efficiency, luminosity and branching fractions. The total systematic uncertainty on $\sigma_{\phi\eta}^{\text{obs}}$, 4.2%, is obtained by summing the individual uncertainties in quadrature.

5 Cross section lineshape of $e^+e^- \rightarrow \phi\eta$

The Born cross section of $e^+e^- \rightarrow \phi\eta$ in the vicinity of the J/ψ resonance, consisting of the continuum and J/ψ resonance contributions, is expressed as [1, 36]:

$$\sigma(s) = \mathcal{P}_{\phi\eta}(s) \cdot \left(\frac{\mathcal{F}}{s^{a_0}} \right)^2 \cdot \frac{4\pi\alpha^2}{3s} \cdot \left| 1 + \frac{3}{\alpha M} \frac{\Gamma_{ee} \cdot (1 + C \cdot e^{i\phi_{\gamma,3g}})}{(s - M^2) + iM\Gamma} \right|^2. \quad (5.1)$$

Here $\mathcal{P}_{\phi\eta}(s)$ is the phase space of the $\phi\eta$ final state expressed as:

$$\mathcal{P}_{\phi\eta}(s) = \left[\frac{(s - M_\phi^2 - M_\eta^2)^2 - 4M_\phi^2M_\eta^2}{s} \right]^{3/2} \quad (5.2)$$

and \mathcal{F}/s^{a_0} is the form factor. We set $a_0 = 1.5$ based on a pQCD theoretical prediction [42]; α is the fine structure constant; M and Γ are the mass and width of the J/ψ meson; Γ_{ee} is the partial width of $J/\psi \rightarrow e^+e^-$; and C is the ratio between $|\mathcal{A}_{3g}|$ and $|\mathcal{A}_\gamma|$.

Due to the effects of ISR and the beam energy spread, the observed cross section cannot be directly compared with the Born cross section. To take into account these effects, a two-fold numerical integration is performed to describe the expected cross section for $e^+e^- \rightarrow \phi\eta$:

$$\sigma^{\text{exp}}(s) = \int_{\sqrt{s}-5S_E}^{\sqrt{s}+5S_E} d\sqrt{s'} G\left(\sqrt{s'}, S_E\right) \int_0^{1-X_{\text{ISR}}} dx F\left(\sqrt{s'}, x\right) \cdot \sigma(s' \cdot (1-x)), \quad (5.3)$$

where $\sqrt{s'}$ is an integration parameter with the dimension of energy; and $G\left(\sqrt{s'}, S_E\right)$ is a Gaussian function to describe the beam energy spread effect with a width of S_E . As explained in section 4.2, X_{ISR} is set as 0.9; and $x = 2E_\gamma/\sqrt{s}$, where E_γ is the energy of radiation

Source	Uncertainty (%)
Luminosity*	1.0
$\mathcal{B}(\phi \rightarrow K^+ K^-)^*$	1.0
$\mathcal{B}(\eta \rightarrow \gamma\gamma)^*$	0.5
Tracking*	2.0
PID*	2.0
Photons reconstruction*	2.0
Kinematic fit*	0.3
Iteration procedure*	0.2
Input lineshape*	1.8
Mass window of $M(\gamma\gamma)^*$	0.0
ϕ fit range	0.4
Signal shape	0.5
Correlated	4.1
Total	4.2

Table 2. Relative systematic uncertainties (in percent) on the observed cross section of $e^+e^- \rightarrow \phi\eta$ at each energy point. Systematic uncertainties for each energy point arise from the efficiency, luminosity and branching fractions. The entry labeled luminosity is the luminosity systematic uncertainty, the two entries labeled $\mathcal{B}(X \rightarrow Y)$ are the branching fraction systematic uncertainties, and everything else is from the efficiency. The sources with star markers are the common and correlated systematic uncertainties.

photon. The ISR function $F(W, x)$ describes the probability of ISR photon emission. From Kuraev and Fadin, it is expressed as [40]:

$$F(W, x) = \beta(1 + \delta)x^{\beta-1} - \beta\left(1 - \frac{x}{2}\right) + \frac{\beta^2}{8} \left[4(2-x)\ln\frac{1}{x} - \frac{1+3(1-x)^2}{x}\ln(1-x) - 6 + x \right], \quad (5.4)$$

with $\delta = \frac{3}{4}\beta + \frac{\alpha}{\pi}\left(\frac{\pi^2}{3} - \frac{1}{2}\right) + \beta^2\left(\frac{9}{32} - \frac{\pi^2}{12}\right)$ and $\beta = \frac{2\alpha}{\pi}\left(2\ln\frac{\sqrt{s}}{m_e} - 1\right)$, where β is the effective bremsstrahlung coupling-constant, and m_e is the invariant mass of electron. We use the analytical formula given in ref. [1] for the subsequent fit to improve the efficiency of the procedure.

The relative phase $\phi_{\gamma,3g}$ and other parameters (\mathcal{F}, C, S_E) are estimated with a least- χ^2 fit to $\sigma_{\phi\eta}^{\text{obs}}$ using the MINUIT package [43]. The χ^2 is built with an effective variance-weighted least squares method, and the correlated systematic uncertainties are considered by the factored minimization method [35]. The χ^2 function reads:

$$\chi^2 = \sum_{i=1}^{26} \frac{(\sigma_{\phi\eta}^{\text{obs}}(s_i) - f \cdot \sigma^{\text{exp}}(s_i))^2}{(\Delta\sigma_{\phi\eta}^{\text{obs}}(s_i))^2 + \left[\frac{1}{2}(\sigma^{\text{exp}}(s_{i,+}) - \sigma^{\text{exp}}(s_{i,-}))\right]^2} + \left(\frac{1-f}{\Delta f}\right)^2 + \sum_{i=1}^3 \left(\frac{P_i^{\text{PDG}} - P_i^{\text{fit}}}{\Delta P_i^{\text{PDG}}}\right)^2. \quad (5.5)$$

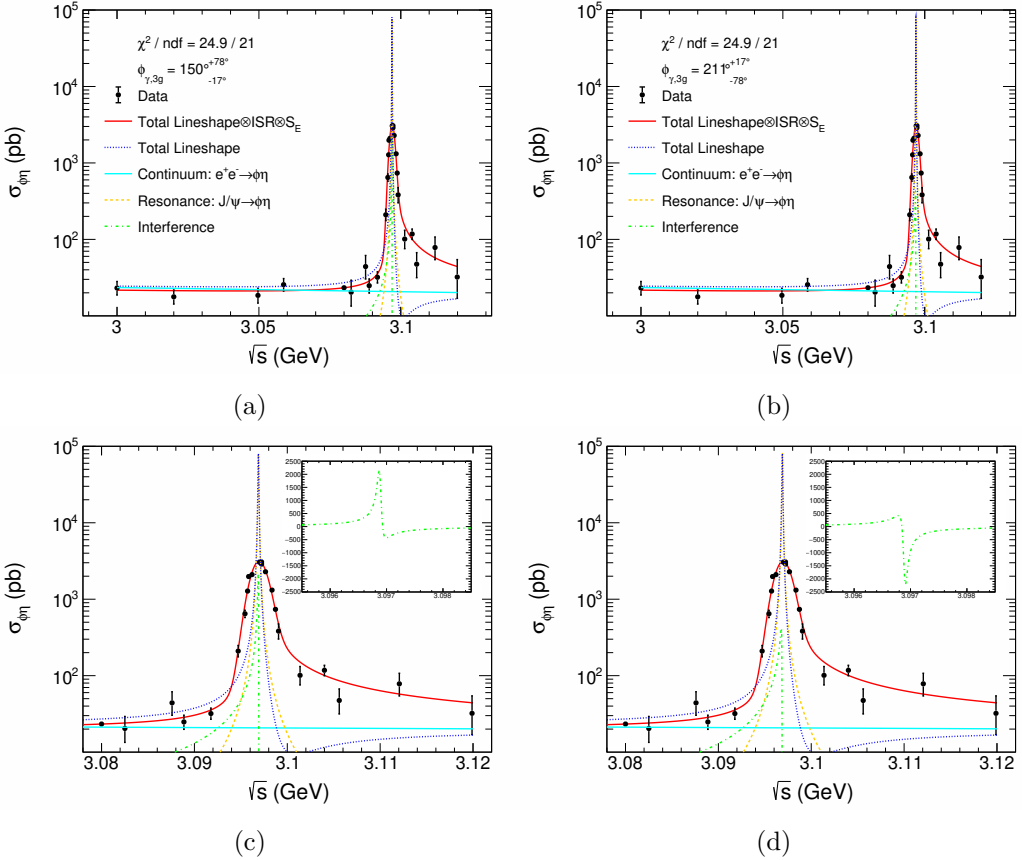


Figure 4. Fit results of the observed cross section lineshape for $e^+e^- \rightarrow \phi\eta$. The left plot is for the positive phase of $\phi_{\gamma,3g}$ and the right for the negative. The black points with error bars are the observed cross section of $e^+e^- \rightarrow \phi\eta$ at each energy point. The solid red curve denotes the overall fit result considering the effects of ISR and beam energy spread. The green solid curve is the lineshape without these two effects. The other curves show the individual contribution of each components without these two effects. The plots (c) and (d) zoom in around the J/ψ resonance peak, providing a more detailed view of the interference patterns in the cross section lineshape for the positive and negative phases, respectively.

In the first term of eq. (5.5), $\Delta\sigma_{\phi\eta}^{\text{obs}}$ is the combined statistical and uncorrelated systematic uncertainties on the $\sigma_{\phi\eta}^{\text{obs}}$ measurement, and $s_{i,\pm} = (\sqrt{s}_i \pm \Delta\sqrt{s}_i)^2$, where $\Delta\sqrt{s}_i$ is the uncertainty of the CM energy measured by the BEMS, and f is a normalization factor introduced as a free parameter to consider the fluctuation on the $\sigma_{\phi\eta}^{\text{obs}}$ measurement caused by the correlated systematic uncertainty Δf in table 2. In the third term, P_i ($i = 1, 2, 3$) represents the parameters for the mass, width, and partial width of the e^+e^- decay mode of the J/ψ meson. These parameters are constrained by considering their uncertainties ΔP_i^{PDG} cited from the PDG [28].

Two separate solutions with positive and negative phases $\phi_{\gamma,3g}$ are found, as shown in figure 4. The fitted parameters are listed in table 3. The uncertainty of the fit result includes both statistical and systematic uncertainties, because all sources of systematic uncertainty have been considered in the χ^2 function. The scanned χ^2 curve is shown in figure 5. As shown in figure 5, these two solutions are indistinguishable within the 1σ confidence interval

	Positive phase	Negative phase
χ^2/ndf	24.9/21	24.9/21
$\phi_{\gamma,3g}$ (°)	150^{+78}_{-17}	211^{+17}_{-78}
\mathcal{F}	0.11 ± 0.01	
C	3.3 ± 0.4	
S_E (MeV)	0.88 ± 0.03	
f	0.99 ± 0.04	

Table 3. Fit results of the lineshape $e^+e^- \rightarrow \phi\eta$. The quoted uncertainties in the fit parameters include both statistical and systematic uncertainties.

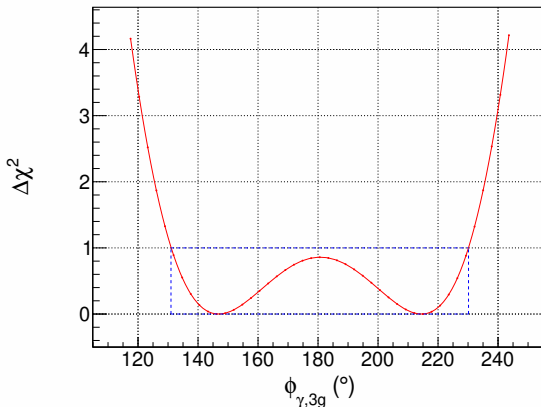


Figure 5. 1D χ^2 -scan over a range of different values for $\phi_{\gamma,3g}$. The dashed blue box represents the interval where $\Delta\chi^2 = \chi^2 - \chi^2_{\min} = 1$, which corresponds to a 1σ confidence interval.

as shown in the dashed-blue box. This results from the non-linear nature of the χ^2 function arising from the low statistics of the data samples. Thus, the relative phase $\phi_{\gamma,3g}$ is measured to be within the range $[133^\circ, 228^\circ]$ within a 1σ confidence interval. The S_E is consistent with the previous analysis reported at BESIII [1].

6 Summary

For the first time, using 26 energy points of e^+e^- annihilation data between 3.00 GeV and 3.12 GeV, with a total integrated luminosity of 452 pb^{-1} , the relative phase between strong and EM amplitudes in the decay $J/\psi \rightarrow VP$ is measured directly through an analysis of the cross section lineshape for $e^+e^- \rightarrow \phi\eta$. The $\phi_{\gamma,3g}$ for $J/\psi \rightarrow \phi\eta$ is determined to be within $[133^\circ, 228^\circ]$ at the 68% confidence level.

Acknowledgments

The BESIII collaboration thanks the staff of BEPCII (<https://cstr.cn/31109.02.BEPC>) and the IHEP computing center for their strong support. This work is supported in part by National Key R&D Program of China under Contracts Nos. 2020YFA0406300, 2020YFA0406400, 2023YFA1606000; National Natural Science Foundation of China (NSFC) under Contracts

Nos. 11635010, 11735014, 11935015, 11935016, 11935018, 12025502, 12035009, 12035013, 12061131003, 12105100, 12192260, 12192261, 12192262, 12192263, 12192264, 12192265, 12221005, 12225509, 12235017, 12361141819; the Chinese Academy of Sciences (CAS) Large-Scale Scientific Facility Program; the CAS Center for Excellence in Particle Physics (CCEPP); Joint Large-Scale Scientific Facility Funds of the NSFC and CAS under Contract No. U1832207; 100 Talents Program of CAS; The Institute of Nuclear and Particle Physics (INPAC) and Shanghai Key Laboratory for Particle Physics and Cosmology; Beijing Municipal Natural Science Foundation under Contracts No. JQ22002; German Research Foundation DFG under Contracts Nos. FOR5327, GRK 2149; Istituto Nazionale di Fisica Nucleare, Italy; Knut and Alice Wallenberg Foundation under Contracts Nos. 2021.0174, 2021.0299; Ministry of Development of Turkey under Contract No. DPT2006K-120470; National Research Foundation of Korea under Contract No. NRF-2022R1A2C1092335; National Science and Technology fund of Mongolia; National Science Research and Innovation Fund (NSRF) via the Program Management Unit for Human Resources & Institutional Development, Research and Innovation of Thailand under Contracts Nos. B16F640076, B50G670107; Polish National Science Centre under Contract No. 2019/35/O/ST2/02907; Swedish Research Council under Contract No. 2019.04595; The Swedish Foundation for International Cooperation in Research and Higher Education under Contract No. CH2018-7756; U.S. Department of Energy under Contract No. DE-FG02-05ER41374.

Data Availability Statement. This article has no associated data or the data will not be deposited.

Code Availability Statement. This article has no associated code or the code will not be deposited.

Open Access. This article is distributed under the terms of the Creative Commons Attribution License ([CC-BY4.0](#)), which permits any use, distribution and reproduction in any medium, provided the original author(s) and source are credited.

References

- [1] BESIII collaboration, *Measurement of the phase between strong and electromagnetic amplitudes of J/ψ decays*, *Phys. Lett. B* **791** (2019) 375 [[arXiv:1808.02166](#)] [[INSPIRE](#)].
- [2] A. Boyarski et al., *The Quantum Numbers and Decay Widths of the $\psi(3095)$* , *Phys. Rev. Lett.* **34** (1975) 1357 [[INSPIRE](#)].
- [3] BES collaboration, *A Measurement of J/ψ decay widths*, *Phys. Lett. B* **355** (1995) 374 [*Erratum ibid.* **363** (1995) 267] [[INSPIRE](#)].
- [4] KEDR collaboration, *Measurement of $\Gamma_{ee}(J/\psi) \cdot \mathcal{B}(J/\psi \rightarrow e^+e^-)$ and $\Gamma_{ee}(J/\psi) \cdot \mathcal{B}(J/\psi \rightarrow \mu^+\mu^-)$* , *Phys. Lett. B* **685** (2010) 134 [[arXiv:0912.1082](#)] [[INSPIRE](#)].
- [5] DM2 collaboration, *The $J/\psi \rightarrow$ Vector + Pseudoscalar Decays and the η, η' Quark Content*, *Phys. Rev. D* **41** (1990) 1389 [[INSPIRE](#)].
- [6] MARK-III collaboration, *Measurements of J/ψ Decays Into a Vector and a Pseudoscalar Meson*, *Phys. Rev. D* **38** (1988) 2695 [*Erratum ibid.* **40** (1989) 3788] [[INSPIRE](#)].

- [7] M. Suzuki, *A large final state interaction in the 0^-0^- decays of J/ψ* , *Phys. Rev. D* **60** (1999) 051501 [[hep-ph/9901327](#)] [[INSPIRE](#)].
- [8] L. Kopke and N. Wermes, *J/ψ Decays*, *Phys. Rep.* **174** (1989) 67 [[INSPIRE](#)].
- [9] M. Suzuki, *Anomalies in $\psi(2S)$ decay and the $\rho\pi$ puzzle*, *Phys. Rev. D* **63** (2001) 054021 [[hep-ph/0006296](#)] [[INSPIRE](#)].
- [10] R. Baldini et al., *Measurement of $J/\psi \rightarrow N\bar{N}$ branching ratios and estimate of the phase of the strong decay amplitude*, *Phys. Lett. B* **444** (1998) 111 [[INSPIRE](#)].
- [11] K. Zhu, X.H. Mo and C.Z. Yuan, *Determination of the relative phase in ψ' and J/ψ decays into baryon and antibaryon*, *Int. J. Mod. Phys. A* **30** (2015) 1550148 [[arXiv:1505.03930](#)] [[INSPIRE](#)].
- [12] CLEO collaboration, *Measurement of interference between electromagnetic and strong amplitudes in $\psi(2S)$ decays to two pseudoscalar mesons*, *Phys. Rev. D* **74** (2006) 011105 [[hep-ex/0603020](#)] [[INSPIRE](#)].
- [13] BESIII collaboration, *Design and Construction of the BESIII Detector*, *Nucl. Instrum. Meth. A* **614** (2010) 345 [[arXiv:0911.4960](#)] [[INSPIRE](#)].
- [14] C. Yu et al., *BEPCII Performance and Beam Dynamics Studies on Luminosity*, in the proceedings of the 7th International Particle Accelerator Conference (IPAC 2016), Busan, South Korea, 8–13 May 2016 [[DOI:10.18429/JACoW-IPAC2016-TUYA01](#)] [[INSPIRE](#)].
- [15] BESIII collaboration, *Future Physics Programme of BESIII*, *Chin. Phys. C* **44** (2020) 040001 [[arXiv:1912.05983](#)] [[INSPIRE](#)].
- [16] J. Lu, Y. Xiao and X. Ji, *Online monitoring of the center-of-mass energy from real data at BESIII*, *Radiat. Detect. Technol. Meth.* **4** (2020) 337 [[INSPIRE](#)].
- [17] J.W. Zhang et al., *Suppression of top-up injection backgrounds with offline event filter in the BESIII experiment*, *Radiat. Detect. Technol. Meth.* **6** (2022) 289 [[INSPIRE](#)].
- [18] X. Li et al., *Study of MRPC technology for BESIII endcap-TOF upgrade*, *Radiat. Detect. Technol. Meth.* **1** (2017) 13 [[INSPIRE](#)].
- [19] Y.X. Guo et al., *The study of time calibration for upgraded end cap TOF of BESIII*, *Radiat. Detect. Technol. Meth.* **1** (2017) 15 [[INSPIRE](#)].
- [20] P. Cao et al., *Design and construction of the new BESIII endcap Time-of-Flight system with MRPC Technology*, *Nucl. Instrum. Meth. A* **953** (2020) 163053 [[INSPIRE](#)].
- [21] E.V. Abakumova et al., *The Beam energy measurement system for the Beijing electron-positron collider*, *Nucl. Instrum. Meth. A* **659** (2011) 21 [[arXiv:1109.5771](#)] [[INSPIRE](#)].
- [22] BESIII collaboration, *Luminosity measurements for the R scan experiment at BESIII*, *Chin. Phys. C* **41** (2017) 063001 [[arXiv:1702.04977](#)] [[INSPIRE](#)].
- [23] GEANT4 collaboration, *GEANT4 — A Simulation Toolkit*, *Nucl. Instrum. Meth. A* **506** (2003) 250 [[INSPIRE](#)].
- [24] S. Jadach, B.F.L. Ward and Z. Was, *Coherent exclusive exponentiation for precision Monte Carlo calculations*, *Phys. Rev. D* **63** (2001) 113009 [[hep-ph/0006359](#)] [[INSPIRE](#)].
- [25] S. Jadach, B.F.L. Ward and Z. Was, *The Precision Monte Carlo event generator KK for two fermion final states in e^+e^- collisions*, *Comput. Phys. Commun.* **130** (2000) 260 [[hep-ph/9912214](#)] [[INSPIRE](#)].
- [26] D.J. Lange, *The EvtGen particle decay simulation package*, *Nucl. Instrum. Meth. A* **462** (2001) 152 [[INSPIRE](#)].

[27] R.G. Ping, *Event generators at BESIII*, *Chin. Phys. C* **32** (2008) 599 [[INSPIRE](#)].

[28] PARTICLE DATA GROUP, *Review of particle physics*, *Phys. Rev. D* **110** (2024) 030001 [[INSPIRE](#)].

[29] J.C. Chen et al., *Event generator for J/ψ and $\psi(2S)$ decay*, *Phys. Rev. D* **62** (2000) 034003 [[INSPIRE](#)].

[30] E. Barberio and Z. Was, *PHOTOS: A Universal Monte Carlo for QED radiative corrections. Version 2.0*, *Comput. Phys. Commun.* **79** (1994) 291 [[INSPIRE](#)].

[31] R.G. Ping, *An exclusive event generator for e^+e^- scan experiments*, *Chin. Phys. C* **38** (2014) 083001 [[arXiv:1309.3932](#)] [[INSPIRE](#)].

[32] BESIII collaboration, *Search for hadronic transition $\chi_{cJ} \rightarrow \eta_c \pi^+ \pi^-$ and observation of $\chi_{cJ} \rightarrow K\bar{K}\pi\pi\pi$* , *Phys. Rev. D* **87** (2013) 012002 [[arXiv:1208.4805](#)] [[INSPIRE](#)].

[33] BESIII collaboration, *Measurement of $e^+e^- \rightarrow \phi\eta'$ cross sections at center-of-mass energies from 3.508 to 4.951 GeV and search for the decay $\psi(3770) \rightarrow \phi\eta'$* , *Phys. Rev. D* **108** (2023) 052015 [[arXiv:2307.12736](#)] [[INSPIRE](#)].

[34] ARGUS collaboration, *Search for Hadronic $b \rightarrow u$ Decays*, *Phys. Lett. B* **241** (1990) 278 [[INSPIRE](#)].

[35] B.P. Roe, *Probability and Statistics in Experimental Physics*, in *Undergraduate Texts in Contemporary Physics (UTCP)*, 2nd edition, Springer, New York, NY, U.S.A. (2001) [[DOI:10.1007/978-1-4684-9296-5](#)].

[36] BABAR collaboration, *Measurements of $e^+e^- \rightarrow K^+K^-\eta$, $K^+K^-\pi^0$ and $K_s^0K^\pm\pi^\mp$ cross-sections using initial state radiation events*, *Phys. Rev. D* **77** (2008) 092002 [[arXiv:0710.4451](#)] [[INSPIRE](#)].

[37] BESIII collaboration, *Study of the process $e^+e^- \rightarrow \phi\eta$ at center-of-mass energies between 2.00 and 3.08 GeV*, *Phys. Rev. D* **104** (2021) 032007 [[arXiv:2104.05549](#)] [[INSPIRE](#)].

[38] BELLE collaboration, *Study of $e^+e^- \rightarrow \eta\phi$ via Initial State Radiation at Belle*, *Phys. Rev. D* **107** (2023) 012006 [[arXiv:2209.00810](#)] [[INSPIRE](#)].

[39] W. Sun et al., *An iterative weighting method to apply ISR correction to e^+e^- hadronic cross-section measurements*, *Front. Phys.* **16** (2021) 64501 [[arXiv:2011.07889](#)] [[INSPIRE](#)].

[40] E.A. Kuraev and V.S. Fadin, *On Radiative Corrections to e^+e^- Single Photon Annihilation at High-Energy*, *Sov. J. Nucl. Phys.* **41** (1985) 466 [[INSPIRE](#)].

[41] Y. Noh, K.K. Choi and L. Du, *Reliability-based design optimization of problems with correlated input variables using a Gaussian Copula*, *Struct. Multidiscip. Optim.* **38** (2008) 1.

[42] C.-D. Lü, W. Wang, Y. Xing and Q.-A. Zhang, *Perturbative QCD analysis of exclusive processes $e^+e^- \rightarrow VP$ and $e^+e^- \rightarrow TP$* , *Phys. Rev. D* **97** (2018) 114016 [[arXiv:1802.09718](#)] [[INSPIRE](#)].

[43] F. James, *MINUIT: Function Minimization and Error Analysis. Reference Manual Version 94.1*, in *CERN Program Library Long Writeup D506*, CERN-D-506, CERN, Geneva, Switzerland (1994) [[INSPIRE](#)].

The BESIII collaboration

M. Ablikim¹, M.N. Achasov^{4,c}, P. Adlarson⁷⁶, O. Afedulidis³, X.C. Ai⁸¹, R. Aliberti³⁵, A. Amoroso^{75A,75C}, Y. Bai⁵⁷, O. Bakina³⁶, I. Balossino^{29A}, Y. Ban^{46,h}, H.-R. Bao⁶⁴, V. Batozskaya^{1,44}, K. Begzsuren³², N. Berger³⁵, M. Berlowski⁴⁴, M. Bertani^{28A}, D. Bettoni^{29A}, F. Bianchi^{75A,75C}, E. Bianco^{75A,75C}, A. Bortone^{75A,75C}, I. Boyko³⁶, R.A. Briere⁵, A. Brueggemann⁶⁹, H. Cai⁷⁷, X. Cai^{1,58}, A. Calcaterra^{28A}, G.F. Cao^{1,64}, N. Cao^{1,64}, S.A. Cetin^{62A}, X.Y. Chai^{46,h}, J.F. Chang^{1,58}, G.R. Che⁴³, Y.Z. Che^{1,58,64}, G. Chelkov^{36,b}, C. Chen⁴³, C.H. Chen⁹, Chao Chen⁵⁵, G. Chen¹, H.S. Chen^{1,64}, H.Y. Chen²⁰, M.L. Chen^{1,58,64}, S.J. Chen⁴², S.L. Chen⁴⁵, S.M. Chen⁶¹, T. Chen^{1,64}, X.R. Chen^{31,64}, X.T. Chen^{1,64}, Y.B. Chen^{1,58}, Y.Q. Chen³⁴, Z.J. Chen^{25,i}, Z.Y. Chen^{1,64}, S.K. Choi¹⁰, G. Cibinetto^{29A}, F. Cossio^{75C}, J.J. Cui⁵⁰, H.L. Dai^{1,58}, J.P. Dai⁷⁹, A. Dbeysi¹⁸, R.E. de Boer³, D. Dedovich³⁶, C.Q. Deng⁷³, Z.Y. Deng¹, A. Denig³⁵, I. Denysenko³⁶, M. Destefanis^{75A,75C}, F. De Mori^{75A,75C}, B. Ding^{1,67}, X.X. Ding^{46,h}, Y. Ding⁴⁰, Y. Ding³⁴, J. Dong^{1,58}, L.Y. Dong^{1,64}, M.Y. Dong^{1,58,64}, X. Dong⁷⁷, M.C. Du¹, S.X. Du⁸¹, Y.Y. Duan⁵⁵, Z.H. Duan⁴², P. Egorov^{36,b}, Y.H. Fan⁴⁵, J. Fang^{1,58}, J. Fang⁵⁹, S.S. Fang^{1,64}, W.X. Fang¹, Y. Fang¹, Y.Q. Fang^{1,58}, R. Farinelli^{29A}, L. Fava^{75B,75C}, F. Feldbauer³, G. Felici^{28A}, C.Q. Feng^{72,58}, J.H. Feng⁵⁹, Y.T. Feng^{72,58}, M. Fritsch³, C.D. Fu¹, J.L. Fu⁶⁴, Y.W. Fu^{1,64}, H. Gao⁶⁴, X.B. Gao⁴¹, Y.N. Gao^{46,h}, Yang Gao^{72,58}, S. Garbolino^{75C}, I. Garzia^{29A,29B}, L. Ge⁸¹, P.T. Ge¹⁹, Z.W. Ge⁴², C. Geng⁵⁹, E.M. Gersabeck⁶⁸, A. Gilman⁷⁰, K. Goetzen¹³, L. Gong⁴⁰, W.X. Gong^{1,58}, W. Gradl³⁵, S. Gramigna^{29A,29B}, M. Greco^{75A,75C}, M.H. Gu^{1,58}, Y.T. Gu¹⁵, C.Y. Guan^{1,64}, A.Q. Guo^{31,64}, L.B. Guo⁴¹, M.J. Guo⁵⁰, R.P. Guo⁴⁹, Y.P. Guo^{12,g}, A. Guskov^{36,b}, J. Gutierrez²⁷, K.L. Han⁶⁴, T.T. Han¹, F. Hanisch³, X.Q. Hao¹⁹, F.A. Harris⁶⁶, K.K. He⁵⁵, K.L. He^{1,64}, F.H. Heinsius³, C.H. Heinz³⁵, Y.K. Heng^{1,58,64}, C. Herold⁶⁰, T. Holtmann³, P.C. Hong³⁴, G.Y. Hou^{1,64}, X.T. Hou^{1,64}, Y.R. Hou⁶⁴, Z.L. Hou¹, B.Y. Hu⁵⁹, H.M. Hu^{1,64}, J.F. Hu^{56,j}, Q.P. Hu^{72,58}, S.L. Hu^{12,g}, T. Hu^{1,58,64}, Y. Hu¹, G.S. Huang^{72,58}, K.X. Huang⁵⁹, L.Q. Huang^{31,64}, X.T. Huang⁵⁰, Y.P. Huang¹, Y.S. Huang⁵⁹, T. Hussain⁷⁴, F. Hölkken³, N. Hüskens³⁵, N. in der Wiesche⁶⁹, J. Jackson²⁷, S. Janchiv³², J.H. Jeong¹⁰, Q. Ji¹, Q.P. Ji¹⁹, W. Ji^{1,64}, X.B. Ji^{1,64}, X.L. Ji^{1,58}, Y.Y. Ji⁵⁰, X.Q. Jia⁵⁰, Z.K. Jia^{72,58}, D. Jiang^{1,64}, H.B. Jiang⁷⁷, P.C. Jiang^{46,h}, S.S. Jiang³⁹, T.J. Jiang¹⁶, X.S. Jiang^{1,58,64}, Y. Jiang⁶⁴, J.B. Jiao⁵⁰, J.K. Jiao³⁴, Z. Jiao²³, S. Jin⁴², Y. Jin⁶⁷, M.Q. Jing^{1,64}, X.M. Jing⁶⁴, T. Johansson⁷⁶, S. Kabana³³, N. Kalantar-Nayestanaki⁶⁵0000-0002-1033-7200, X.L. Kang⁹, X.S. Kang⁴⁰, M. Kavatsyuk⁶⁵, B.C. Ke⁸¹, V. Khachatryan²⁷, A. Khoukaz⁶⁹, R. Kiuchi¹, O.B. Kolcu^{62A}, B. Kopf³, M. Kuessner³, X. Kui^{1,64}, N. Kumar²⁶, A. Kupsc^{44,76}, W. Kühn³⁷, L. Lavezzi^{75A,75C}, T.T. Lei^{72,58}, Z.H. Lei^{72,58}, M. Lellmann³⁵, T. Lenz³⁵, C. Li⁴⁷, C. Li⁴³, C.H. Li³⁹, Cheng Li^{72,58}, D.M. Li⁸¹, F. Li^{1,58}, G. Li¹, H.B. Li^{1,64}, H.J. Li¹⁹, H.N. Li^{56,j}, Hui Li⁴³, J.R. Li⁶¹, J.S. Li⁵⁹, K. Li¹, K.L. Li¹⁹, L.J. Li^{1,64}, L.K. Li¹, Lei Li⁴⁸, M.H. Li⁴³, P.R. Li^{38,k,l}, Q.M. Li^{1,64}, Q.X. Li⁵⁰, R. Li^{17,31}, S.X. Li¹², T. Li⁵⁰, W.D. Li^{1,64}, W.G. Li^{1,a}, X. Li^{1,64}, X.H. Li^{72,58}, X.L. Li⁵⁰, X.Y. Li^{1,8}, X.Z. Li⁵⁹, Y.G. Li^{46,h}, Z.J. Li⁵⁹, Z.Y. Li⁷⁹, C. Liang⁴², H. Liang^{72,58}, Hao Liang^{1,64}, Y.F. Liang⁵⁴, Y.T. Liang^{31,64}, G.R. Liao¹⁴, Y.P. Liao^{1,64}, J. Libby²⁶, A. Limphirat⁶⁰, C.C. Lin⁵⁵, C.X. Lin⁶⁴, D.X. Lin^{31,64}, T. Lin¹, B.J. Liu¹, B.X. Liu⁷⁷, C. Liu³⁴,

C.X. Liu $\textcolor{red}{\text{#1}}$, F. Liu $\textcolor{red}{\text{#1}}$, F.H. Liu $\textcolor{red}{\text{#53}}$, Feng Liu $\textcolor{red}{\text{#6}}$, G.M. Liu $\textcolor{red}{\text{#56,}j}$, H. Liu $\textcolor{red}{\text{#38,}k,l}$, H.B. Liu $\textcolor{red}{\text{#15}}$,
 H.H. Liu $\textcolor{red}{\text{#1}}$, H.M. Liu $\textcolor{red}{\text{#1,}64}$, Huihui Liu $\textcolor{red}{\text{#21}}$, J.B. Liu $\textcolor{red}{\text{#72,}58}$, J.Y. Liu $\textcolor{red}{\text{#1,}64}$, K. Liu $\textcolor{red}{\text{#38,}k,l}$,
 K.Y. Liu $\textcolor{red}{\text{#40}}$, Ke Liu $\textcolor{red}{\text{#22}}$, L. Liu $\textcolor{red}{\text{#72,}58}$, L.C. Liu $\textcolor{red}{\text{#43}}$, Lu Liu $\textcolor{red}{\text{#43}}$, M.H. Liu $\textcolor{red}{\text{#12,}g}$, P.L. Liu $\textcolor{red}{\text{#1}}$,
 Q. Liu $\textcolor{red}{\text{#64}}$, S.B. Liu $\textcolor{red}{\text{#72,}58}$, T. Liu $\textcolor{red}{\text{#12,}g}$, W.K. Liu $\textcolor{red}{\text{#43}}$, W.M. Liu $\textcolor{red}{\text{#72,}58}$, X. Liu $\textcolor{red}{\text{#38,}k,l}$, X. Liu $\textcolor{red}{\text{#39}}$,
 Y. Liu $\textcolor{red}{\text{#38,}k,l}$, Y. Liu $\textcolor{red}{\text{#81}}$, Y.B. Liu $\textcolor{red}{\text{#43}}$, Z.A. Liu $\textcolor{red}{\text{#1,}58,}64$, Z.D. Liu $\textcolor{red}{\text{#9}}$, Z.Q. Liu $\textcolor{red}{\text{#50}}$,
 X.C. Lou $\textcolor{red}{\text{#1,}58,}64$, F.X. Lu $\textcolor{red}{\text{#59}}$, H.J. Lu $\textcolor{red}{\text{#23}}$, J.G. Lu $\textcolor{red}{\text{#1,}58}$, X.L. Lu $\textcolor{red}{\text{#1}}$, Y. Lu $\textcolor{red}{\text{#7}}$, Y.P. Lu $\textcolor{red}{\text{#1,}58}$,
 Z.H. Lu $\textcolor{red}{\text{#1,}64}$, C.L. Luo $\textcolor{red}{\text{#41}}$, J.R. Luo $\textcolor{red}{\text{#59}}$, M.X. Luo $\textcolor{red}{\text{#80}}$, T. Luo $\textcolor{red}{\text{#12,}g}$, X.L. Luo $\textcolor{red}{\text{#1,}58}$, X.R. Lyu $\textcolor{red}{\text{#64}}$,
 Y.F. Lyu $\textcolor{red}{\text{#43}}$, F.C. Ma $\textcolor{red}{\text{#40}}$, H. Ma $\textcolor{red}{\text{#79}}$, H.L. Ma $\textcolor{red}{\text{#1}}$, J.L. Ma $\textcolor{red}{\text{#1,}64}$, L.L. Ma $\textcolor{red}{\text{#50}}$, L.R. Ma $\textcolor{red}{\text{#67}}$,
 M.M. Ma $\textcolor{red}{\text{#1,}64}$, Q.M. Ma $\textcolor{red}{\text{#1}}$, R.Q. Ma $\textcolor{red}{\text{#1,}64}$, T. Ma $\textcolor{red}{\text{#72,}58}$, X.T. Ma $\textcolor{red}{\text{#1,}64}$, X.Y. Ma $\textcolor{red}{\text{#1,}58}$,
 Y.M. Ma $\textcolor{red}{\text{#31}}$, F.E. Maas $\textcolor{red}{\text{#18}}$, I. MacKay $\textcolor{red}{\text{#70}}$, M. Maggiора $\textcolor{red}{\text{#75A,}75C}$, S. Malde $\textcolor{red}{\text{#70}}$, Y.J. Mao $\textcolor{red}{\text{#46,}h}$,
 Z.P. Mao $\textcolor{red}{\text{#1}}$, S. Marcello $\textcolor{red}{\text{#75A,}75C}$, Z.X. Meng $\textcolor{red}{\text{#67}}$, J.G. Messchendorp $\textcolor{red}{\text{#13,}65}$, G. Mezzadri $\textcolor{red}{\text{#29A}}$,
 H. Miao $\textcolor{red}{\text{#1,}64}$, T.J. Min $\textcolor{red}{\text{#42}}$, R.E. Mitchell $\textcolor{red}{\text{#27}}$, X.H. Mo $\textcolor{red}{\text{#1,}58,}64$, B. Moses $\textcolor{red}{\text{#27}}$, N. Yu. Muchnoi $\textcolor{red}{\text{#4,}c}$,
 J. Muskalla $\textcolor{red}{\text{#35}}$, Y. Nefedov $\textcolor{red}{\text{#36}}$, F. Nerling $\textcolor{red}{\text{#18,}e}$, L.S. Nie $\textcolor{red}{\text{#20}}$, I.B. Nikolaev $\textcolor{red}{\text{#4,}c}$, Z. Ning $\textcolor{red}{\text{#1,}58}$,
 S. Nisar $\textcolor{red}{\text{#11,}m}$, Q.L. Niu $\textcolor{red}{\text{#38,}k,l}$, W.D. Niu $\textcolor{red}{\text{#55}}$, Y. Niu $\textcolor{red}{\text{#50}}$, S.L. Olsen $\textcolor{red}{\text{#10,}64}$, Q. Ouyang $\textcolor{red}{\text{#1,}58,}64$,
 S. Pacetti $\textcolor{red}{\text{#28B,}28C}$, X. Pan $\textcolor{red}{\text{#55}}$, Y. Pan $\textcolor{red}{\text{#57}}$, A. Pathak $\textcolor{red}{\text{#34}}$, Y.P. Pei $\textcolor{red}{\text{#72,}58}$, M. Pelizaeus $\textcolor{red}{\text{#3}}$,
 H.P. Peng $\textcolor{red}{\text{#72,}58}$, Y.Y. Peng $\textcolor{red}{\text{#38,}k,l}$, K. Peters $\textcolor{red}{\text{#13,}e}$, J.L. Ping $\textcolor{red}{\text{#41}}$, R.G. Ping $\textcolor{red}{\text{#1,}64}$, S. Plura $\textcolor{red}{\text{#35}}$,
 V. Prasad $\textcolor{red}{\text{#33}}$, F.Z. Qi $\textcolor{red}{\text{#1}}$, H. Qi $\textcolor{red}{\text{#72,}58}$, H.R. Qi $\textcolor{red}{\text{#61}}$, M. Qi $\textcolor{red}{\text{#42}}$, T.Y. Qi $\textcolor{red}{\text{#12,}g}$, S. Qian $\textcolor{red}{\text{#1,}58}$,
 W.B. Qian $\textcolor{red}{\text{#64}}$, C.F. Qiao $\textcolor{red}{\text{#64}}$, X.K. Qiao $\textcolor{red}{\text{#81}}$, J.J. Qin $\textcolor{red}{\text{#73}}$, L.Q. Qin $\textcolor{red}{\text{#14}}$, L.Y. Qin $\textcolor{red}{\text{#72,}58}$,
 X.P. Qin $\textcolor{red}{\text{#12,}g}$, X.S. Qin $\textcolor{red}{\text{#50}}$, Z.H. Qin $\textcolor{red}{\text{#1,}58}$, J.F. Qiu $\textcolor{red}{\text{#1}}$, Z.H. Qu $\textcolor{red}{\text{#73}}$, C.F. Redmer $\textcolor{red}{\text{#35}}$,
 K.J. Ren $\textcolor{red}{\text{#39}}$, A. Rivetti $\textcolor{red}{\text{#75C}}$, M. Rolo $\textcolor{red}{\text{#75C}}$, G. Rong $\textcolor{red}{\text{#1,}64}$, Ch. Rosner $\textcolor{red}{\text{#18}}$, M.Q. Ruan $\textcolor{red}{\text{#1,}58}$,
 S.N. Ruan $\textcolor{red}{\text{#43}}$, N. Salone $\textcolor{red}{\text{#44}}$, A. Sarantsev $\textcolor{red}{\text{#36,}d}$, Y. Schelhaas $\textcolor{red}{\text{#35}}$, K. Schoenning $\textcolor{red}{\text{#76}}$,
 M. Scodeggio $\textcolor{red}{\text{#29A}}$, K.Y. Shan $\textcolor{red}{\text{#12,}g}$, W. Shan $\textcolor{red}{\text{#24}}$, X.Y. Shan $\textcolor{red}{\text{#72,}58}$, Z.J. Shang $\textcolor{red}{\text{#38,}k,l}$,
 J.F. Shangguan $\textcolor{red}{\text{#16}}$, L.G. Shao $\textcolor{red}{\text{#1,}64}$, M. Shao $\textcolor{red}{\text{#72,}58}$, C.P. Shen $\textcolor{red}{\text{#12,}g}$, H.F. Shen $\textcolor{red}{\text{#1,}8}$,
 W.H. Shen $\textcolor{red}{\text{#64}}$, X.Y. Shen $\textcolor{red}{\text{#1,}64}$, B.A. Shi $\textcolor{red}{\text{#64}}$, H. Shi $\textcolor{red}{\text{#72,}58}$, J.L. Shi $\textcolor{red}{\text{#12,}g}$, J.Y. Shi $\textcolor{red}{\text{#1}}$,
 Q.Q. Shi $\textcolor{red}{\text{#55}}$, S.Y. Shi $\textcolor{red}{\text{#73}}$, X. Shi $\textcolor{red}{\text{#1,}58}$, J.J. Song $\textcolor{red}{\text{#19}}$, T.Z. Song $\textcolor{red}{\text{#59}}$, W.M. Song $\textcolor{red}{\text{#1,}34}$,
 Y.J. Song $\textcolor{red}{\text{#12,}g}$, Y.X. Song $\textcolor{red}{\text{#46,}h,n}$, S. Sosio $\textcolor{red}{\text{#75A,}75C}$, S. Spataro $\textcolor{red}{\text{#75A,}75C}$, F. Stieler $\textcolor{red}{\text{#35}}$, S.S. Su $\textcolor{red}{\text{#40}}$,
 Y.J. Su $\textcolor{red}{\text{#64}}$, G.B. Sun $\textcolor{red}{\text{#77}}$, G.X. Sun $\textcolor{red}{\text{#1}}$, H. Sun $\textcolor{red}{\text{#64}}$, H.K. Sun $\textcolor{red}{\text{#1}}$, J.F. Sun $\textcolor{red}{\text{#19}}$, K. Sun $\textcolor{red}{\text{#61}}$,
 L. Sun $\textcolor{red}{\text{#77}}$, S.S. Sun $\textcolor{red}{\text{#1,}64}$, T. Sun $\textcolor{red}{\text{#51,}f}$, W.Y. Sun $\textcolor{red}{\text{#34}}$, Y. Sun $\textcolor{red}{\text{#9}}$, Y.J. Sun $\textcolor{red}{\text{#72,}58}$, Y.Z. Sun $\textcolor{red}{\text{#1}}$,
 Z.Q. Sun $\textcolor{red}{\text{#1,}64}$, Z.T. Sun $\textcolor{red}{\text{#50}}$, C.J. Tang $\textcolor{red}{\text{#54}}$, G.Y. Tang $\textcolor{red}{\text{#1}}$, J. Tang $\textcolor{red}{\text{#59}}$, M. Tang $\textcolor{red}{\text{#72,}58}$,
 Y.A. Tang $\textcolor{red}{\text{#77}}$, L.Y. Tao $\textcolor{red}{\text{#73}}$, Q.T. Tao $\textcolor{red}{\text{#25,}i}$, M. Tat $\textcolor{red}{\text{#70}}$, J.X. Teng $\textcolor{red}{\text{#72,}58}$, V. Thoren $\textcolor{red}{\text{#76}}$,
 W.H. Tian $\textcolor{red}{\text{#59}}$, Y. Tian $\textcolor{red}{\text{#31,}64}$, Z.F. Tian $\textcolor{red}{\text{#77}}$, I. Uman $\textcolor{red}{\text{#62B}}$, Y. Wan $\textcolor{red}{\text{#55}}$, S.J. Wang $\textcolor{red}{\text{#50}}$,
 B. Wang $\textcolor{red}{\text{#1}}$, B.L. Wang $\textcolor{red}{\text{#64}}$, Bo Wang $\textcolor{red}{\text{#72,}58}$, D.Y. Wang $\textcolor{red}{\text{#46,}h}$, F. Wang $\textcolor{red}{\text{#73}}$, H.J. Wang $\textcolor{red}{\text{#38,}k,l}$,
 J.J. Wang $\textcolor{red}{\text{#77}}$, J.P. Wang $\textcolor{red}{\text{#50}}$, K. Wang $\textcolor{red}{\text{#1,}58}$, L.L. Wang $\textcolor{red}{\text{#1}}$, M. Wang $\textcolor{red}{\text{#50}}$, N.Y. Wang $\textcolor{red}{\text{#64}}$,
 S. Wang $\textcolor{red}{\text{#12,}g}$, S. Wang $\textcolor{red}{\text{#38,}k,l}$, T. Wang $\textcolor{red}{\text{#12,}g}$, T.J. Wang $\textcolor{red}{\text{#43}}$, W. Wang $\textcolor{red}{\text{#59}}$, Wei Wang $\textcolor{red}{\text{#73}}$,
 W.P. Wang $\textcolor{red}{\text{#35,}72,}58,o$, X. Wang $\textcolor{red}{\text{#46,}h}$, X.F. Wang $\textcolor{red}{\text{#38,}k,l}$, X.J. Wang $\textcolor{red}{\text{#39}}$, X.L. Wang $\textcolor{red}{\text{#12,}g}$,
 X.N. Wang $\textcolor{red}{\text{#1}}$, Y. Wang $\textcolor{red}{\text{#61}}$, Y.D. Wang $\textcolor{red}{\text{#45}}$, Y.F. Wang $\textcolor{red}{\text{#1,}58,}64$, Y.H. Wang $\textcolor{red}{\text{#38,}k,l}$, Y.L. Wang $\textcolor{red}{\text{#19}}$,
 Y.N. Wang $\textcolor{red}{\text{#45}}$, Y.Q. Wang $\textcolor{red}{\text{#1}}$, Yaqian Wang $\textcolor{red}{\text{#17}}$, Yi Wang $\textcolor{red}{\text{#61}}$, Z. Wang $\textcolor{red}{\text{#1,}58}$, Z.L. Wang $\textcolor{red}{\text{#73}}$,
 Z.Y. Wang $\textcolor{red}{\text{#1,}64}$, Ziyi Wang $\textcolor{red}{\text{#64}}$, D.H. Wei $\textcolor{red}{\text{#14}}$, F. Weidner $\textcolor{red}{\text{#69}}$, S.P. Wen $\textcolor{red}{\text{#1}}$, Y.R. Wen $\textcolor{red}{\text{#39}}$,
 U. Wiedner $\textcolor{red}{\text{#3}}$, G. Wilkinson $\textcolor{red}{\text{#70}}$, M. Wolke $\textcolor{red}{\text{#76}}$, L. Wollenberg $\textcolor{red}{\text{#3}}$, C. Wu $\textcolor{red}{\text{#39}}$, J.F. Wu $\textcolor{red}{\text{#1,}8}$,
 L.H. Wu $\textcolor{red}{\text{#1}}$, L.J. Wu $\textcolor{red}{\text{#1,}64}$, X. Wu $\textcolor{red}{\text{#12,}g}$, X.H. Wu $\textcolor{red}{\text{#34}}$, Y. Wu $\textcolor{red}{\text{#72,}58}$, Y.H. Wu $\textcolor{red}{\text{#55}}$, Y.J. Wu $\textcolor{red}{\text{#31}}$,
 Z. Wu $\textcolor{red}{\text{#1,}58}$, L. Xia $\textcolor{red}{\text{#72,}58}$, X.M. Xian $\textcolor{red}{\text{#39}}$, B.H. Xiang $\textcolor{red}{\text{#1,}64}$, T. Xiang $\textcolor{red}{\text{#46,}h}$, D. Xiao $\textcolor{red}{\text{#38,}k,l}$,
 G.Y. Xiao $\textcolor{red}{\text{#42}}$, S.Y. Xiao $\textcolor{red}{\text{#1}}$, Y.L. Xiao $\textcolor{red}{\text{#12,}g}$, Z.J. Xiao $\textcolor{red}{\text{#41}}$, C. Xie $\textcolor{red}{\text{#42}}$, X.H. Xie $\textcolor{red}{\text{#46,}h}$, Y. Xie $\textcolor{red}{\text{#50}}$,
 Y.G. Xie $\textcolor{red}{\text{#1,}58}$, Y.H. Xie $\textcolor{red}{\text{#6}}$, Z.P. Xie $\textcolor{red}{\text{#72,}58}$, T.Y. Xing $\textcolor{red}{\text{#1,}64}$, C.F. Xu $\textcolor{red}{\text{#1,}64}$, C.J. Xu $\textcolor{red}{\text{#59}}$, G.F. Xu $\textcolor{red}{\text{#1}}$,

H.Y. Xu^{12,67}, M. Xu^{12,58}, Q.J. Xu¹⁶, Q.N. Xu³⁰, W. Xu¹, W.L. Xu⁶⁷, X.P. Xu⁵⁵,
 Y. Xu⁴⁰, Y.C. Xu⁷⁸, Z.S. Xu⁶⁴, F. Yan^{12,g}, L. Yan^{12,g}, W.B. Yan^{72,58}, W.C. Yan⁸¹,
 X.Q. Yan^{1,64}, H.J. Yang^{51,f}, H.L. Yang³⁴, H.X. Yang¹, J.H. Yang⁴², T. Yang¹,
 Y. Yang^{12,g}, Y.F. Yang^{1,64}, Y.F. Yang⁴³, Y.X. Yang^{1,64}, Z.W. Yang^{38,k,l}, Z.P. Yao⁵⁰,
 M. Ye^{1,58}, M.H. Ye⁸, J.H. Yin¹, Junhao Yin⁴³, Z.Y. You⁵⁹, B.X. Yu^{1,58,64}, C.X. Yu⁴³,
 G. Yu^{1,64}, J.S. Yu^{25,i}, M.C. Yu⁴⁰, T. Yu⁷³, X.D. Yu^{46,h}, Y.C. Yu⁸¹, C.Z. Yuan^{1,64},
 J. Yuan³⁴, J. Yuan⁴⁵, L. Yuan², S.C. Yuan^{1,64}, Y. Yuan^{1,64}, Z.Y. Yuan⁵⁹, C.X. Yue³⁹,
 A.A. Zafar⁷⁴, F.R. Zeng⁵⁰, S.H. Zeng⁶³, X. Zeng^{12,g}, Y. Zeng^{25,i}, Yujie Zeng⁵⁹,
 Y.J. Zeng^{1,64}, X.Y. Zhai³⁴, Y.C. Zhai⁵⁰, Y.H. Zhan⁵⁹, A.Q. Zhang^{1,64}, B.L. Zhang^{1,64},
 B.X. Zhang¹, D.H. Zhang⁴³, G.Y. Zhang¹⁹, H. Zhang^{72,58}, H. Zhang⁸¹,
 H.C. Zhang^{1,58,64}, H.H. Zhang⁵⁹, H.H. Zhang³⁴, H.Q. Zhang^{1,58,64}, H.R. Zhang^{72,58},
 H.Y. Zhang^{1,58}, Jin Zhang⁸¹, J. Zhang⁵⁹, J.J. Zhang⁵², J.L. Zhang²⁰, J.Q. Zhang⁴¹,
 J.S. Zhang^{12,g}, J.W. Zhang^{1,58,64}, J.X. Zhang^{38,k,l}, J.Y. Zhang¹, J.Z. Zhang^{1,64},
 Jianyu Zhang⁶⁴, L.M. Zhang⁶¹, Lei Zhang⁴², P. Zhang^{1,64}, Q.Y. Zhang³⁴,
 R.Y. Zhang^{38,k,l}, S.H. Zhang^{1,64}, Shulei Zhang^{25,i}, X.M. Zhang¹, X.Y. Zhang⁴⁰,
 X.Y. Zhang⁵⁰, Y. Zhang¹, Y. Zhang⁷³, Y.T. Zhang⁸¹, Y.H. Zhang^{1,58}, Y.M. Zhang³⁹,
 Yan Zhang^{72,58}, Z.D. Zhang¹, Z.H. Zhang¹, Z.L. Zhang³⁴, Z.Y. Zhang⁷⁷, Z.Y. Zhang⁴³,
 Z.Z. Zhang⁴⁵, G. Zhao¹, J.Y. Zhao^{1,64}, J.Z. Zhao^{1,58}, L. Zhao¹, Lei Zhao^{72,58},
 M.G. Zhao⁴³, N. Zhao⁷⁹, R.P. Zhao⁶⁴, S.J. Zhao⁸¹, Y.B. Zhao^{1,58}, Y.X. Zhao^{31,64},
 Z.G. Zhao^{72,58}, A. Zhemchugov^{36,b}, B. Zheng⁷³, B.M. Zheng³⁴, J.P. Zheng^{1,58},
 W.J. Zheng^{1,64}, Y.H. Zheng⁶⁴, B. Zhong⁴¹, X. Zhong⁵⁹, H. Zhou⁵⁰, J.Y. Zhou³⁴,
 L.P. Zhou^{1,64}, S. Zhou⁶, X. Zhou⁷⁷, X.K. Zhou⁶, X.R. Zhou^{72,58}, X.Y. Zhou³⁹,
 Y.Z. Zhou^{12,g}, Z.C. Zhou²⁰, A.N. Zhu⁶⁴, J. Zhu⁴³, K. Zhu¹, K.J. Zhu^{1,58,64},
 K.S. Zhu^{12,g}, L. Zhu³⁴, L.X. Zhu⁶⁴, S.H. Zhu⁷¹, T.J. Zhu^{12,g}, W.D. Zhu⁴¹,
 Y.C. Zhu^{72,58}, Z.A. Zhu^{1,64}, J.H. Zou¹, J. Zu^{72,58}

¹ Institute of High Energy Physics, Beijing 100049, People's Republic of China

² Beihang University, Beijing 100191, People's Republic of China

³ Bochum Ruhr-University, D-44780 Bochum, Germany

⁴ Budker Institute of Nuclear Physics SB RAS (BINP), Novosibirsk 630090, Russia

⁵ Carnegie Mellon University, Pittsburgh, Pennsylvania 15213, USA

⁶ Central China Normal University, Wuhan 430079, People's Republic of China

⁷ Central South University, Changsha 410083, People's Republic of China

⁸ China Center of Advanced Science and Technology, Beijing 100190, People's Republic of China

⁹ China University of Geosciences, Wuhan 430074, People's Republic of China

¹⁰ Chung-Ang University, Seoul, 06974, Republic of Korea

¹¹ COMSATS University Islamabad, Lahore Campus, Defence Road, Off Raiwind Road, 54000 Lahore, Pakistan

¹² Fudan University, Shanghai 200433, People's Republic of China

¹³ GSI Helmholtzcentre for Heavy Ion Research GmbH, D-64291 Darmstadt, Germany

¹⁴ Guangxi Normal University, Guilin 541004, People's Republic of China

¹⁵ Guangxi University, Nanning 530004, People's Republic of China

¹⁶ Hangzhou Normal University, Hangzhou 310036, People's Republic of China

¹⁷ Hebei University, Baoding 071002, People's Republic of China

¹⁸ Helmholtz Institute Mainz, Staudinger Weg 18, D-55099 Mainz, Germany

¹⁹ Henan Normal University, Xinxiang 453007, People's Republic of China

²⁰ Henan University, Kaifeng 475004, People's Republic of China

²¹ Henan University of Science and Technology, Luoyang 471003, People's Republic of China

²² Henan University of Technology, Zhengzhou 450001, People's Republic of China
²³ Huangshan College, Huangshan 245000, People's Republic of China
²⁴ Hunan Normal University, Changsha 410081, People's Republic of China
²⁵ Hunan University, Changsha 410082, People's Republic of China
²⁶ Indian Institute of Technology Madras, Chennai 600036, India
²⁷ Indiana University, Bloomington, Indiana 47405, USA
²⁸ INFN Laboratori Nazionali di Frascati, (A)INFN Laboratori Nazionali di Frascati, I-00044, Frascati, Italy;
 (B)INFN Sezione di Perugia, I-06100, Perugia, Italy; (C)University of Perugia, I-06100, Perugia, Italy
²⁹ INFN Sezione di Ferrara, (A)INFN Sezione di Ferrara, I-44122, Ferrara, Italy; (B)University of Ferrara,
 I-44122, Ferrara, Italy
³⁰ Inner Mongolia University, Hohhot 010021, People's Republic of China
³¹ Institute of Modern Physics, Lanzhou 730000, People's Republic of China
³² Institute of Physics and Technology, Peace Avenue 54B, Ulaanbaatar 13330, Mongolia
³³ Instituto de Alta Investigación, Universidad de Tarapacá, Casilla 7D, Arica 1000000, Chile
³⁴ Jilin University, Changchun 130012, People's Republic of China
³⁵ Johannes Gutenberg University of Mainz, Johann-Joachim-Becher-Weg 45, D-55099 Mainz, Germany
³⁶ Joint Institute for Nuclear Research, 141980 Dubna, Moscow region, Russia
³⁷ Justus-Liebig-Universitaet Giessen, II. Physikalisches Institut, Heinrich-Buff-Ring 16, D-35392 Giessen,
 Germany
³⁸ Lanzhou University, Lanzhou 730000, People's Republic of China
³⁹ Liaoning Normal University, Dalian 116029, People's Republic of China
⁴⁰ Liaoning University, Shenyang 110036, People's Republic of China
⁴¹ Nanjing Normal University, Nanjing 210023, People's Republic of China
⁴² Nanjing University, Nanjing 210093, People's Republic of China
⁴³ Nankai University, Tianjin 300071, People's Republic of China
⁴⁴ National Centre for Nuclear Research, Warsaw 02-093, Poland
⁴⁵ North China Electric Power University, Beijing 102206, People's Republic of China
⁴⁶ Peking University, Beijing 100871, People's Republic of China
⁴⁷ Qufu Normal University, Qufu 273165, People's Republic of China
⁴⁸ Renmin University of China, Beijing 100872, People's Republic of China
⁴⁹ Shandong Normal University, Jinan 250014, People's Republic of China
⁵⁰ Shandong University, Jinan 250100, People's Republic of China
⁵¹ Shanghai Jiao Tong University, Shanghai 200240, People's Republic of China
⁵² Shanxi Normal University, Linfen 041004, People's Republic of China
⁵³ Shanxi University, Taiyuan 030006, People's Republic of China
⁵⁴ Sichuan University, Chengdu 610064, People's Republic of China
⁵⁵ Soochow University, Suzhou 215006, People's Republic of China
⁵⁶ South China Normal University, Guangzhou 510006, People's Republic of China
⁵⁷ Southeast University, Nanjing 211100, People's Republic of China
⁵⁸ State Key Laboratory of Particle Detection and Electronics, Beijing 100049, Hefei 230026, People's
 Republic of China
⁵⁹ Sun Yat-Sen University, Guangzhou 510275, People's Republic of China
⁶⁰ Suranaree University of Technology, University Avenue 111, Nakhon Ratchasima 30000, Thailand
⁶¹ Tsinghua University, Beijing 100084, People's Republic of China
⁶² Turkish Accelerator Center Particle Factory Group, (A)Istanbul University, 34010, Istanbul, Turkey;
 (B)Near East University, Nicosia, North Cyprus, 99138, Mersin 10, Turkey
⁶³ University of Bristol, H H Wills Physics Laboratory, Tyndall Avenue, Bristol, BS8 1TL, UK
⁶⁴ University of Chinese Academy of Sciences, Beijing 100049, People's Republic of China
⁶⁵ University of Groningen, NL-9747 AA Groningen, The Netherlands
⁶⁶ University of Hawaii, Honolulu, Hawaii 96822, USA
⁶⁷ University of Jinan, Jinan 250022, People's Republic of China
⁶⁸ University of Manchester, Oxford Road, Manchester, M13 9PL, United Kingdom
⁶⁹ University of Muenster, Wilhelm-Klemm-Strasse 9, 48149 Muenster, Germany

⁷⁰ University of Oxford, Keble Road, Oxford OX13RH, United Kingdom
⁷¹ University of Science and Technology Liaoning, Anshan 114051, People's Republic of China
⁷² University of Science and Technology of China, Hefei 230026, People's Republic of China
⁷³ University of South China, Hengyang 421001, People's Republic of China
⁷⁴ University of the Punjab, Lahore-54590, Pakistan
⁷⁵ University of Turin and INFN, (A) University of Turin, I-10125, Turin, Italy; (B) University of Eastern Piedmont, I-15121, Alessandria, Italy; (C) INFN, I-10125, Turin, Italy
⁷⁶ Uppsala University, Box 516, SE-75120 Uppsala, Sweden
⁷⁷ Wuhan University, Wuhan 430072, People's Republic of China
⁷⁸ Yantai University, Yantai 264005, People's Republic of China
⁷⁹ Yunnan University, Kunming 650500, People's Republic of China
⁸⁰ Zhejiang University, Hangzhou 310027, People's Republic of China
⁸¹ Zhengzhou University, Zhengzhou 450001, People's Republic of China

^a Deceased

^b Also at the Moscow Institute of Physics and Technology, Moscow 141700, Russia

^c Also at the Novosibirsk State University, Novosibirsk, 630090, Russia

^d Also at the NRC "Kurchatov Institute", PNPI, 188300, Gatchina, Russia

^e Also at Goethe University Frankfurt, 60323 Frankfurt am Main, Germany

^f Also at Key Laboratory for Particle Physics, Astrophysics and Cosmology, Ministry of Education; Shanghai Key Laboratory for Particle Physics and Cosmology; Institute of Nuclear and Particle Physics, Shanghai 200240, People's Republic of China

^g Also at Key Laboratory of Nuclear Physics and Ion-beam Application (MOE) and Institute of Modern Physics, Fudan University, Shanghai 200443, People's Republic of China

^h Also at State Key Laboratory of Nuclear Physics and Technology, Peking University, Beijing 100871, People's Republic of China

ⁱ Also at School of Physics and Electronics, Hunan University, Changsha 410082, China

^j Also at Guangdong Provincial Key Laboratory of Nuclear Science, Institute of Quantum Matter, South China Normal University, Guangzhou 510006, China

^k Also at MOE Frontiers Science Center for Rare Isotopes, Lanzhou University, Lanzhou 730000, People's Republic of China

^l Also at Lanzhou Center for Theoretical Physics, Lanzhou University, Lanzhou 730000, People's Republic of China

^m Also at the Department of Mathematical Sciences, IBA, Karachi 75270, Pakistan

ⁿ Also at Ecole Polytechnique Federale de Lausanne (EPFL), CH-1015 Lausanne, Switzerland

^o Also at Helmholtz Institute Mainz, Staudinger Weg 18, D-55099 Mainz, Germany